Pacific Northwest
NATIONAL LABORATORY

PNNL-30541

Characterization of Radiation Induced Defects Across Scales

September 2020

Lucas E. Sweet
Jordan F. Corbey
Matteo Leoni

U.S. DEPARTMENT OF ENERGY

Prepared for the U.S. Department of Energy
under Contract DE-AC05-76RL01830

DISCLAIMER

PACIFIC NORTHWEST NATIONAL LABORATORY
operated by
BATTELLE
for the
UNITED STATES DEPARTMENT OF ENERGY
under Contract DE-AC05-76RL01830

Printed in the United States of America

Available to DOE and DOE contractors from the
Office of Scientific and Technical Information,
P.O. Box 62, Oak Ridge, TN 37831-0062;
ph: (865) 576-8401
fax: (865) 576-5728
email: reports@adonis.osti.gov

Available to the public from the National Technical Information Service
5301 Shawnee Rd., Alexandria, VA 22312
ph: (800) 553-NTIS (6847)
email: orders@ntis.gov <https://www.ntis.gov/about>
Online ordering: http://www.ntis.gov

PNNL-30541

Characterization of Radiation Induced Defects Across Scales

September 2020

Lucas E. Sweet
Jordan F. Corbey
Matteo Leoni

Prepared for
the U.S. Department of Energy
under Contract DE-AC05-76RL01830

Pacific Northwest National Laboratory
Richland, Washington 99354

Crystallite Size Distributions of PuO_2 from Whole Powder Pattern Modelling of X-Ray Diffraction Data

Authors

Lucas Sweet[a]*, Jordan Corbey[a] and Matteo Leoni[b]
[a]Nuclear Process Signatures, Pacific Northwest National Laboratory, 902 Battelle Blvd., Richland, WA, 99352, United States
[b] University of Trento, Mesiano, 77, Trento, 38123, Italy

Correspondence email: lucas.sweet@pnnl.gov

Abstract The Whole Powder Pattern Modelling (WPPM) approach of diffraction line profile analysis (LPA) was applied for the first time on PuO_2 in order to understand the evolution of the microstructural properties as a function of process conditions. Crystallite size distributions and defect concentrations were determined by WPPM on three different PuO_2 samples - including one with a bimodal distribution and compared to the result of more common LPA analyses used in PuO_2 literature studies (e.g. Scherrer equation, double Voigt method). The conclusion was that a lognormal distribution of spherical crystallites with dislocations most closely represent the microstructure of PuO_2 produced by heating $Pu_2(C_2O_4)_3(H_2O)_6 \cdot 3H_2O$ between 650°C and 850°C. The volume-weighted mean column length (L_{vol}) parameter obtained from the double Voigt method for the monomodal samples were the same as the L_{vol} obtained from the WPPM within uncertainty. The two LPA methods did not agree on the L_{vol} parameters of the bimodal distribution sample with only the WPPM getting values that were consistent with the individual components. The WPPM can potentially provide more insight into future studies of the influences on the microstructure properties of PuO_2

1. Introduction

The microstructure of PuO_2 has been studied since the Manhattan era and is still a focus today, although our drivers have changed. Today we are interested in how the micr-structural properties of PuO_2, including various colloidal hydrolysis products, impact environmental fate and transport of particulates for environmental clean up sites and waste repositories.(Delegard, 2013; Hixon & Powell, 2018; Kersting, 2013) In addition, performance and safety testing associated with proposed uses of mixed oxide nuclear fuels in power reactors, as a route for plutonium disposition, also rely on accurate measurements of microstructural properties of PuO_2.(Cina, 1963; Machuron-Mandard & Madic, 1996) In the vein of national security, there have been indications that the microstructural properties of PuO_2 could be of significance in nuclear forensics technologies.(Mayer *et al.*, 2013) Due to the hazards, value, and rarity of plutonium samples, there is motivation to maximize the amount of useful information one can obtain from a minimal number of measurements.

Diffraction line profile analysis (LPA) for the purpose of quantifying microstructural properties has evolved significantly over the period of time in which PuO_2 has been studied. Early methods included what is commonly referred to as the Scherrer equation(Scherrer, 1918) the Warren-Averbach method(Warren & Averbach, 1950) and Williamson-Hall plot(Williamson & Hall, 1953) deconvolution methods. Each of these methods applies a unique set of assumptions and definitions of the microstructure properties they report. Past studies of PuO_2, in

most cases, employ approximated line profiles based on analytical functions (like Gaussian, Voigt, etc.) that are mathematically convenient, but are just approximations of the true shapes resulting from microstructure properties. The simplicity of using analytical functions to quantify microstructural properties could come at the cost of accuracy.

With the history of microstructure characterization by LPA in mind, we have evaluated the available literature that re-ports microstructural properties of PuO_2 and find that, in every case, some level of approximation is used to obtain a "crystallite size," generally reported as a single value.(Machuron-Mandard & Madic, 1996; Smith *et al.*, 1976; Kanellakopulos *et al.*, 1983) In many cases, the methods used to obtain the crystallite size value were not described well enough to know the definition of "crystallite size" that was used. Standards to account for instrument contributions to peak shape were rarely used, often because they were not available at the time. The combination of lacking information such as instrument standards used and definitions of terms used for line profile analysis makes comparisons of past studies and current studies extremely difficult.

Today, with a variety of LPA methods available in various easy to use software packages, as well as rigorously validated standard reference materials, it is worth some effort to evaluate the options for LPA when it comes to studies of transuranic materials. The Whole Powder Pattern Modelling (WPPM), as most recently outlined and generalized by Scardi and Leoni,(Scardi *et al.*, 2000; Scardi & Leoni, 2002; Leoni *et al.*, 2004) has gained a lot of attention and has been generally regarded as the preferred method when accuracy is considered important.(Mittemeijer *et al.*, 2004) One of the drawbacks of WPPM is that it can take a considerable amount of work to get suitable models for different systems. In the case of PuO_2, WPPM can be applied with minimal model development effort since much validation work has been done with CeO_2, a reasonable surrogate for PuO_2. This work outlines our efforts to apply the WPPM method of LPA to quantify the microstructural properties of PuO_2 prepared under different conditions. We also compare results obtained from the double Voigt method(Snyder *et al.*, 1999) of whole powder pattern fitting (WPPF) to those obtained from WPPM.

In an effort to make the results from this study useful to others in the future, we are following four key guidelines to reporting LPA results:

1) Define the models/methods used for the LPA
2) Define assumptions made in the models/methods
3) Define the calibration method used to account for instrument profile and/or other validations needed to make the results as instrumentation independent as possible
4) Report the raw data with data collection detail

2. Methods

All radioactive samples were prepared at a non-reactor nuclear facility by certified and trained personnel inside of a glove box designed for contamination control. Three samples of $^{239}PuO_2$ were generated to have distinctly different crystallite size distributions. Sample 1 was made by heating plutonium (III) oxalate (confirmed to be $Pu_2(C_2O_4)_3(H_2O)_6 \cdot 3H_2O$ by powder X-ray diffraction)(Runde *et al.*, 2009) at 650°C for 2 hours in a box furnace. Sample 2 was made by taking a portion of Sample 1 and heat treating it at 850°C for 2 hours. Sample 3 was made by

mixing a portion of Sample 1 and a portion of Sample 2 together to create a roughly 50:50 mixture.

Each powder X-ray diffraction (PXRD) sample was prepared in a poly(methyl methacrylate) plastic sample holder with a 25 mm diameter by 1 mm deep sample well (Bruker part #C79298A3244D97). Each holder was covered with a 8 μm thick polyimide film (SPEX SamplePrep #3512) that was secured in place with a plastic snap ring. Each sample configuration was removed from the glove box and determined to be free of external radioactive material contamination with assistance of a radiation control technician and radiation detection equipment before being placed on the X-ray diffractometer.

PXRD data were collected for Samples 1 and 3 using a Rigaku Ultima IV diffractometer equipped with a Cu sealed tube X-ray source, using a divergent slit of 1/2°, a height limiting slit of 10 mm, 5° Soller slits on the source and detector sides, a 2/3° scattering slit, a 0.15 mm receiving slit, a bent graphite monochromator on the detector side and a scintillation detector on a 285 mm radius goniometer. Diffraction data were collected on Sample 2 using the same diffractometer and settings except that a 1/3° divergent slit was used. Data were collected from 20-140° 2θ in 0.01° increments with a scan rate of 0.14 degrees per minute for all samples. Data were collected also for NIST SRM 660c in order to determine the zero error and instrument contribution to the diffraction peak profiles. The same diffractometer and data collection settings were used for SRM 660c as those used for the PuO_2 samples. The raw diffraction data collected for each sample and SRM 660c using the two different divergent slit settings are included in the Supplemental Information.

The diffraction data for Samples 1-3 were analysed using both the double Voigt WPPF method implemented in TOPAS v6 software package(*TOPAS*, 2016) and the WPPM method implemented in PM2K.(Leoni *et al.*, 2006) For these LPA methods, we consider instrument contributions to broadening, crystallite (aka coherently scattering domain) size broadening and broadening from dislocations. The two methods, double Voigt WPPF and WPPM, use different functions to represent each source of broadening, and those are described below.

For the WPPM analysis, the model chosen to represent our instrument contribution to the line profile is the Caglioti model(Caglioti *et al.*, 1958) and as stated above the model was fit to a diffraction pattern of the NIST SRM 660c (LaB_6). The model used to account for the contribution to the profile broadening from the finite small size of the coherently scattering domains (crystallites) considers a log normal distribution of spherical crystallites in the specimen, as shown in equation 1.

$$g_l(D) = \frac{1}{D\sigma\sqrt{2\pi}} e^{-\frac{(lnD-\mu)^2}{2\sigma^2}} \qquad \text{eq 1}$$

where D is the crystallite diameter, μ is the lognormal mean and σ the lognormal variance. The model used to account for profile broadening caused by microstrain, ε (Δd/d), as a result of dislocations was the Wilkens-Krivoglaz model.(Krivoglaz & Ryaboshapka, 1963; Wilkens, 1970) The Wilkens-Krivoglaz model relates the mean square strain $\langle \varepsilon^2_{(hkl)} \rangle$ to the concentration of dislocations, ρ, the average contrast factor, $\bar{C}_{(hkl)}$, the Burgers vector, b, for a slip system $\langle UVW \rangle (HKL)$, and the average cut off radius, R_e, shown in equation 2

$$\langle \varepsilon^2_{(hkl)} \rangle = \frac{\rho \bar{C}_{(hkl)} b^2}{4\pi} f^* \left(\frac{L}{R_e} \right) \qquad \text{eq 2}$$

where f^* is the Wilkens function.(Simmons *et al.*, 1970) For face centred cubic (fcc) structures, the lowest-energy slip system is $\langle 110 \rangle (111)$, as illustrated in Figure 2. The Burgers vector for this system is $\frac{a}{\sqrt{2}}$. The average contrast factor $\bar{C}_{(hkl)}$. accounts for the anisotropy of the strain field of the dislocations that results in a peculiar trend of the breadth and shape of the line profiles in the pattern, sometimes referred to as the "visibility" of a dislocation. The contrast factor is a function of the single-crystal elastic constants and the symmetry of the lattice and its calculation can be tedious, but there are some helpful guides that have been published.(Borbely *et al.*, 2003; Martinez-Garcia *et al.*, 2009; Scardi, Ortolani, *et al.*, 2010; Ungar & Tichy, 1999) The character of the dislocations is considered in an effective way in the contrast factor through the weighting factor f_{mix}:

$$\bar{C}_{(hkl)} = [f_{mix}A_E + (1 - f_{mix}A_S)] + [f_{mix}B_E + (1 - f_{mix}B_S)]\left[\frac{h^2k^2+k^2l^2+l^2h^2}{(h^2+k^2+l^2)^2}\right] \qquad \text{eq 3}$$

where A_E, A_S, B_E and B_S are the contrast coefficients associated with pure edge (E subscript) and pure screw (S subscript) dislocations. For PuO_2, the contrast coefficients, calculated according to the procedure outlined by Martinez-Garcia et al.,(Martinez-Garcia *et al.*, 2009) using the single-crystal elastic constants c_{11} = 320, c_{12} = 178 and c_{44} = 75 published by Zhang, P. et. al.,(Zhang *et al.*, 2010) are A_E = 0.190, B_E = 0.014, A_S = 0.171 and B_s = 0.190.

The double Voigt method falls into the category of Whole Powder Pattern Fitting (WPPF) techniques, since arbitrary analytical functions are employed to represent broadening from the finite size of crystallites and from microstrain. The fundamental parameters method described by Cheary and Coelho(Cheary & Coelho, 1992) to account for instrument broadening was used. The crystallite size and microstrain broadening were represented by a Lorentzian and Gaussian function, respectively. The integral breadth of the Lorentzian function, β_{IB}, was used to calculate a volume weighted mean column length, L_{vol}, as shown in equation 4, and the full width at half maximum of the Gaussian function, β_{FWHM}, is used to calculate the microstrain parameter ε, as show in equation 5.

$$L_{vol-IB} = \frac{\lambda}{\beta_{IB}cos\theta} \qquad \text{eq 4}$$

$$\varepsilon = \frac{\beta_{FWHM}}{4tan\theta} \qquad \text{eq 5}$$

The bimodal distribution model used for Sample 3, which is a mix of PuO_2 heated at 650°C and PuO_2 heated at 850°C, consisted of two PuO_2 phases with independently refined unit cell parameters, lognormal spherical crystallite diameter distributions and defect concentrations using the Wilkens model described above. The intensities of the peaks for the two phases were constrained by a single scale factor, "k" so that the peak intensities for component 1 were multiplied by k, and the peak intensities of component 2 were multiplied by 1-k. The scale factor was constrained to refine between 0 and 1. Since no structure factors were used in the WPPM refinements, the use of the scale factor assures that all peaks in each phase get the appropriate relative intensities proportional to the concentration of each PuO_2 component in the mixture.

3. Results and Discussion

WPPM uses physically meaningful models to represent microstructural contributions to diffraction line profiles. However, in the absence of any complementary information about the material's microstructural properties, some assumptions need to be made. For this work, since we had no additional information apart from what powder X-ray diffraction (PXRD) data could provide about the microstructural properties of the PuO2 samples prepared, we made 3 assumptions: 1) the crystallites are spherical in shape; 2) the distribution of crystallite sizes is lognormal in nature; 3) dis-locations are present in PuO2. We made some attempts to support these assumptions which we describe below.

3.1. Support for Assumption 1.

The size values obtained from traditional LPA methods cannot be directly related to data collected using a complementary technique such as transmission electron microscopy (TEM), as they represent different averages. The TEM can provide crystallite shape information and assess, at least qualitatively, the uniformity of that shape. At the time of this study, we did not have the ability to analyse these PuO2 samples using TEM or any other technique to confirm the crystallite shape. Diffraction can provide this information indirectly, as the shape of the crystallites affects the shape of the peaks. In particular, the presence of an isotropic size broadening is an indication of an average spherical shape. Vice versa, a peculiar anisotropy in the broadening would result when the shape is not spherical. We did evaluate the observed diffraction patterns with models for other crystallite shapes such as spheres, cubes, tetrahedrons, octahedrons and cylinders, and the results from these different models are shown in Figure 1. The sphere shape (with a lognormal size distribution) provides the best agreement factor (Rwp) and is also visually the one that better fit the measured data. This is consistent with re-sults obtained from a similar study of CeO2 which included TEM analysis.(Leoni *et al.*, 2004; Vella *et al.*, 2006) Additionally, we applied a WPPF method that allowed for the anisotropic refinement of spheroid shape crystallites with three independently refined axes to define the shape, and an isotropic shape (sphere) resulted in the best fit.(Ectors *et al.*, 2015a, b) The same refinement was performed for a cuboid shape defined by two freely refined axes, and a cube was the best fit but had a larger R_{wp} value than the sphere. Because of the results from these tests, the spherical shape was chosen to represent the crystallites in the PuO2 specimens used in this study.

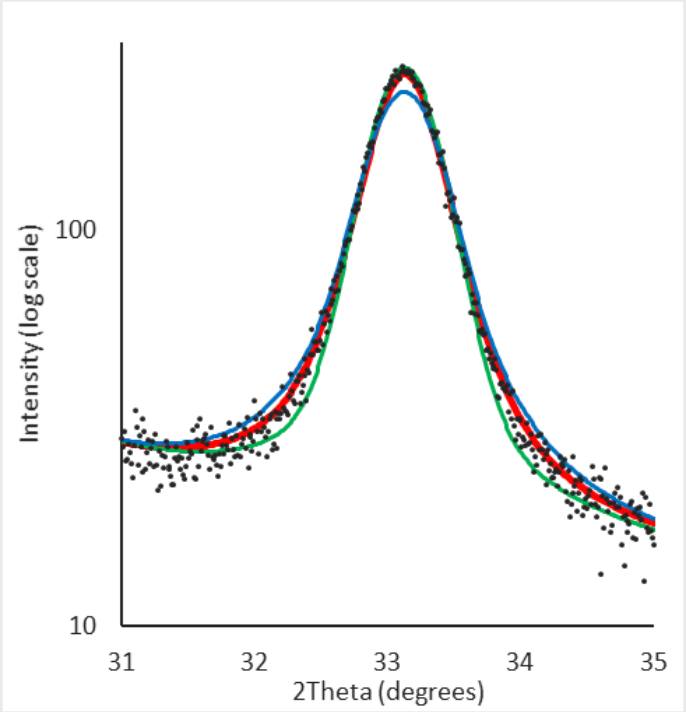

Figure 1 Zoomed view of the (200) peak of Sample 1, PuO2 heated at 650°C, to show the results of the different crystallite shape model fits to the whole pattern using WPPM. The black dots correspond to the observed diffraction data. The coloured lines correspond to the different crystallite shape model fits: red is the spherical model fit (R_{wp} 8.83%), green is the cube model fit (R_{wp} 9.19%), blue is the tetrahedron fit (10.02%). Not shown are the octahedron and cylinder model fits which resulted in residuals of R_{wp} = 9.20% and 12.6%, respectively.

3.2. Support for Assumption 2.

Materials generally have a distribution of crystallite sizes that affects the peak shape. It is possible to refine a histogram distribution of crystallite sizes, but this adds a lot of variables in the refinement and, consequently, instability. A logical first choice for a crystallite size distribution for PuO_2 produced as described above is a lognormal distribution, shown in equation 1. Much like the evaluation of crystallite shape, we do not have any complementary analysis data to inform us of the possible distribution shapes, but we did try out several others such a gamma distribution and a York distribution, shown in equations 6 and 7, respectively. These three distributions were tested with each of the five tested crystallite shapes (sphere, cube, tetrahedron, octahedron and cylinder), and the best fit was obtained with a lognormal distribution of spheres. This result is also consistent with more thorough investigations of CeO_2.(Leoni *et al.*, 2004; Scardi, Leoni, *et al.*, 2010)

$$g(D) = \frac{\sigma}{\mu\Gamma(\sigma)}\left(\frac{\sigma D}{\mu}\right)^{\sigma-1} e^{-\frac{\sigma D}{\mu}} \qquad \text{eq 6}$$

$$g(D) = \frac{\sigma}{\mu\Gamma(\sigma)}\left(\frac{\sigma D}{\mu}\right)^{\sigma} e^{-\frac{\sigma D}{\mu}} \qquad \text{eq 7}$$

1. Support for Assumption 3.

We again have no complementary analyses of microstructural properties for these specimens apart from the diffraction ones. We do have the knowledge from other reported works that the Wilkens model is appropriate to describe dislocations for face centered cubic (fcc) oxides similar to PuO_2.(Mittemeijer *et al.*, 2004; Scardi, Leoni, *et al.*, 2010) In this work, the introduction of dislocations in the modeling results in an improvement of the fit supported by the decrease in R_{wp} from 9.54% to 8.83%. The presence of other types of defects,(Warren, 1969) albeit possible, cannot be inferred from the data, as no residual broadening is evident.

A shift in the unit cell parameter was observed between Sample 1 and Sample 2 which could be attributed to several effects, Frenkel pairs being one of them, but non-stoichiometry in PuO_2 seems to be a more common attribution to unit cell shifts.(Weber, 1984) The refined unit cell parameters for Samples 1 and 2 are 5.4021(1) Å and 5.3956(1) Å, respectively. Variation in the refined lattice parameters from replicate data acquisitions of NIST SRM 660c, collected around the same time as the PuO_2 samples, was $\pm 4.16 \times 10^{-5}$ Å, so we view the difference in the refined unit cell parameter for these two PuO_2 samples (0.0065 Å) as significant. If we use the relationship between unit cell parameter and O:Pu ratio reported by Haschke, Allen and Morales,(Haschke *et al.*, 2000) then the chemical formula for Sample 1 (PuO_2 heated at 650° C) should be $PuO_{2.17}$, and the formula for Sample 2 (PuO_2 heated at 850° C) should be $PuO_{1.79}$. The reported unit cell parameter from Belin, R. C.; et. al.(Belin *et al.*, 2004) is 5.39819(1) Å and from Zachariasen, W. H.,(Zachariasen, 1949) is 5.397(1) Å.

While it is not possible to evaluate every model combination for defects and crystallite size distribution, we can make these reasonable assumptions and support them with the limited observations available to us. Plutonium materials science tends to be plagued with limited analysis modalities because of the hazards associated with the material. By identifying which LPA methods and models are used and providing supporting evidence for these selections, results can be more clearly evaluated, and gaps in knowledge can be identified. For example, in this study, TEM analysis to support the choice of crystallite shape and defect types would help to support the validity of the results. The WPPM method forces some thought to be put into exactly how the line profiles are evaluated and sets the framework for a more comprehensive microstructure evaluation when one attempts to eliminate assumptions with complementary analyses.

As mentioned above, the Wilkens model did improve the overall model fit to the observed data in the WPPM refinements, as seen in Figure 2; the presence of dislocations is reasonable for an oxide with the fluorite structure type,(Ashbee & Frank, 1970) and nuclear reactions are known to increase the dislocation content. Fixing the cutoff radius at a reasonable distance, say 5 nm, the dislocation density drops to 8.7×10^{15} m^{-2} (1 dislocation in 1.2×10^3 nm^2), which is less than 1 defect per cross sectional area of a mean sized crystallite (66 nm^2). A similar behaviour was obtained when the Wilkens model was applied to Sample 2. We therefore believe dislocations are present in PuO_2 and they can be sensed. This can have a high value for studies related to the degradation of nuclear fuels and of materials exposed to nuclear irradiation. The density is however too low here for an accurate quantification. The crystallite size distribution for these samples was not impacted by the incorporation of this dislocation model indicating a low correlation between these model parameters. The refined dislocation densities ρ, for Samples 1 and 2 are reported in Table 1.

In order to compare the results from WPPM to those obtained by WPPF, the L_{vol} (volume weighted mean column length) needs to be calculated from the refined WPPM size distribution parameters. The relationship between L_{vol} and the lognormal distribution parameters μ and σ is shown in equation 8:(Scardi & Leoni, 2001; Kril & Birringer, 1998)

$$\langle L \rangle_{vol} = \frac{3}{4} e^{\mu + \frac{7}{2}\sigma^2} \qquad \text{eq 8}$$

Both μ and σ in this equation are equal to the same definition as used in Table 1 and above.

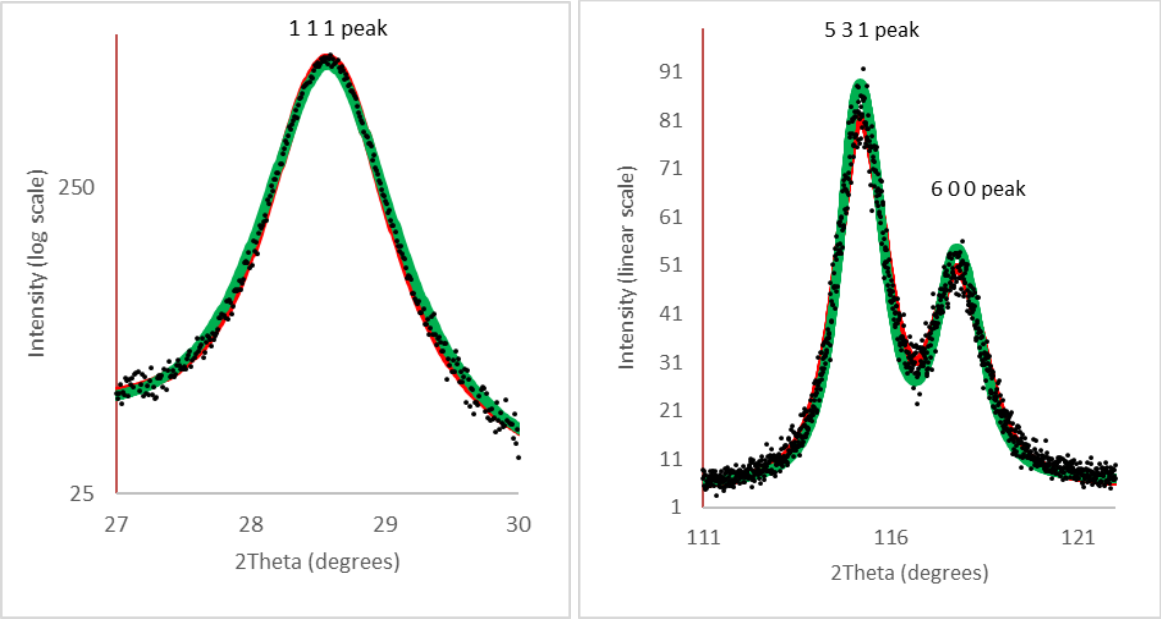

Figure 2 The fit of the model with the slip system convolution (red line, R_{wp} 8.83%) and without (green line, R_{wp} 9.54%) to the observed diffraction data (black dots) for a few of the peaks in the pattern for Sample 1.

As seen in Table 1, the $L_{vol\text{-}IB}$ values obtained from the double Voigt WPPF method agree with the L_{vol} values obtained from WPPM for sample 1 but tend to depart for Sample 2. The reason for this difference can be found in Figure 3, presenting the size distributions obtained for the two specimens. Sample 2 has a much broader and skewed distribution and the signal from the larger crystallites (larger volume fraction), tend to dominate of the signal of the smaller ones. This is a further reason to prefer analytical methods that interpret the whole profile physically, with respect to methods that just fit it in order to obtain an accurate breadth information.

Table 1 Results of WPPM and WPPF refinements for Samples 1 and 2.

Parameter	Sample 1 (PuO_2 heated at 650°C)	Sample 2 (PuO_2 heated at 850°C)
μ	2.02(3)	3.29(3)

σ	0.460(9)	0.49(1)
ρ (m^{-2})	$1.8(1)x10^{15}$	$5.78(2)x10^{11}$
R_e defect cutoff radius (nm)	4(2)	5 (fixed)
L_{vol} from WPPM (nm)	11.9(7)	47(4)
L_{area} from WPPM (nm)	8.5(4)	33(2)
$L_{vol\text{-}IB}$ from WPPF (nm)	11.86(5)	52.1(2)
e^o microstrain from WPPF	$1.16x10^{-3}$	$2.5x10^{-4}$

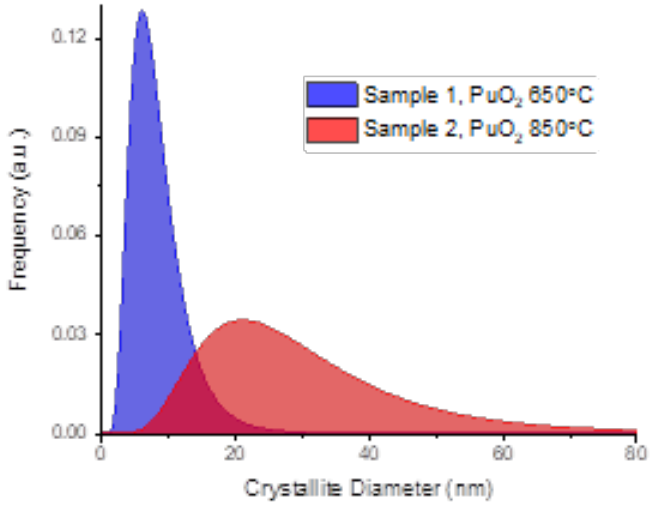

Figure 3 The distribution of diameters of spherical crystallites as determined by the WPPM refinement of Sample 1 (PuO_2 heated at 650°C), tan, and Sample 2 (PuO_2 heated at 850°C), blue.

We further tested the limits of the LPA methods by analyzing a sample that is designed to have a bimodal distribution of crystallite sizes. Sample 3, the mixture of Samples 1 and 2, could not be fit well with a model for a single lognormal distribution of crystallites of any shape, as seen in Figure 4. The bimodal distribution model gave a better fit both upon visual inspection, see Figure 4, and with an improved R_{wp} value by 1.48%, as shown in Table 2.

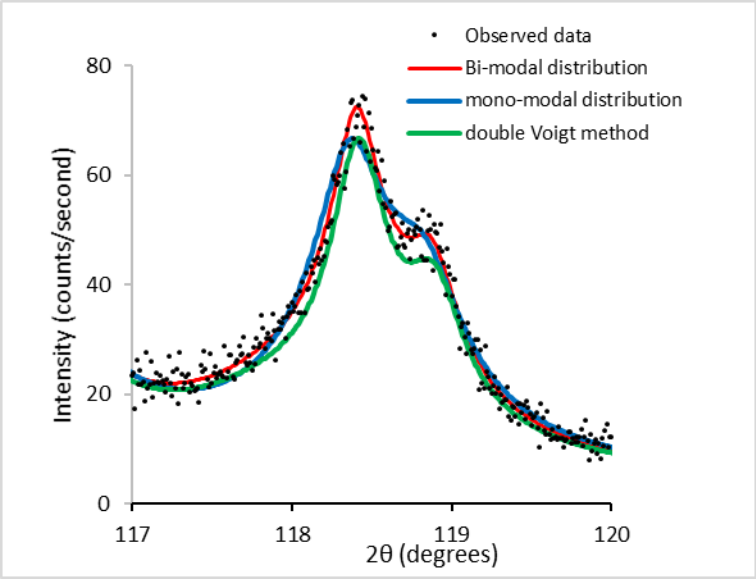

Figure 4 The fit of the WPPM bi-modal distribution model, red line, compared to that of the WPPM mono-modal distribution model, blue line, and the WPPF 2 component double Voigt method fit, green line, to the observed data, black dots, for the (442) reflection.

Table 2 Refined parameters from WPPM and WPPF LPA of Sample 3, a mixture of Sample 1 (PuO_2 heated to 650°C) and Sample 2 (PuO_2 heated to 850°C).

Parameter	Bi-modal model fit	Mono-modal model fit
μ	Comp 1: 2.11(9), Comp 2: 3.30(7)	0.70(6)
σ	Comp 1: 0.45(6) Comp 2: 0.46(1)	0.89(1)
ρ (m^{-2})	Comp 1: 2.1(2) x10^{15} Comp 2: N/A	4.7(5)x10^{14}
R_e defect cutoff radius (nm)	Comp 1: 5 (fixed) Comp 2: N/A	5 (fixed)
L_{vol} from WPPM (nm)	Comp 1: 13(4) Comp 2: 43(4)	24
L_{vol} from WPPF (nm)	Comp 1: 13.1(1) Comp 2: 34.4(6)	18.7(1)
Unit cell parameter: a (Å)	Comp 1: 5.4031(2) Comp 2: 5.3957(1)	5.3974(1)
Composition (wt. %)	Comp 1: 59% Comp 2: 41%	N/A
R_{wp} WPPM	9.12%	10.6%
R_{wp} WPPF	10.21%	12.45%

All of the refinement values for component 1 and component 2 in the bimodal distribution model, shown in Table 2, were very similar, and in most cases identical within the uncertainty values, to the WPPM refinement values of Sample 1 and Sample 2, indicating that WPPM can be quite consistent even for mixed phases with overlapping peaks. As in the case of Sample 2, the dislocation density for component 2 in the bi-modal distribution model refined to a value that was unreasonably small. The resulting crystallite size distributions for each of the components used in the bimodal distribution model and the overall distribution are plotted in Figure 5.

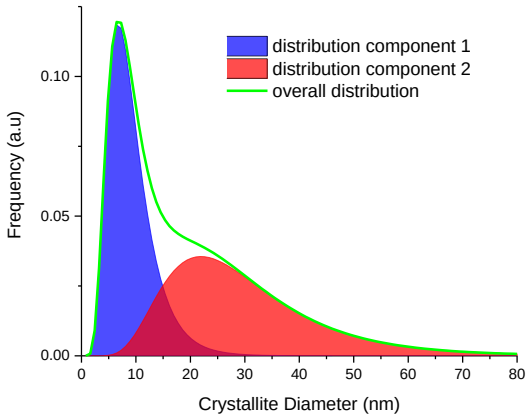

Figure 5 The overall bimodal distribution of spherical crystallite diameters for Sample 3 (mixture of PuO_2 heated to 650°C and 850°C, respectively) is shown as the green line. The two components that make up the overall distribution (blue and red curves) are very similar to the distributions of Sample 1 and 2 (shown in Figure 3).

As a further test of the uniqueness of the microstructure values that were obtained from the WPPM method, we used the same bimodal distribution model constructed for Sample 3 on the data collected for Sample 1 (PuO_2 heated to 650°C). This resulted in one component refining to the same values as those obtained when using just a single component model and the other component refining to a distribution of nonsensically small crystallites (L_{vol} = 0.05 nm). The k factor indicated that the sample was composed nearly entirely of the component that contained the crystallite size distribution and defect concentration identical to that obtained for the mono-modal distribution.

A two-component model was also used with the double Voigt WPPF method for a comparison. The resulting fit from the double Voigt method was not quite as good as the two-component model using the WPPM method, as can be seen by the green trace in Figure 4, being a bit too narrow as compared to the observed data. As seen in Table 2, the L_{vol} value obtained from the double Voigt WPPF method for component 1 matches that of Sample 1 using the same method, but the L_{vol} value for component 2 is significantly smaller than that of Sample 2.

2. Conclusions

In response to a desire to compile and establish trends in the evolution of PuO_2 microstructure properties as a function of process conditions, we found the need to evaluate the accuracy of PXRD LPA techniques. The WPPM method was applied to the LPA of PXRD data collected for 3 samples, and the results were compared to the LPA by the more commonly used double Voigt method. While the two LPA methods produce L_{vol} values that agree within error for the two samples that appear to be fit well with mono-modal crystallite size distributions, the WPPM method provides a more useful and complete picture of the microstructure properties by describing the distribution of crystallites and dislocation densities. For the bimodal distribution sample (Sample 3), the benefit of using physically meaningful profile convolutions in the WPPM method became even more clear as this method was able to accurately identify and quantify the microstructure properties of the two components used to make the mixture, whereas the double

Voigt WPPF method did not produce results that were as close to the expected L_{vol} values for the individual components.

The hope here is to outline an approach to the quantification of microstructural properties of rarely studied materials so that the results can be clearly interpreted, evaluated and potentially reinterpreted well after the material is accessible. To this end, we have included the raw diffraction data for the three samples in addition to the raw diffraction data collected from NIST SRM 660c using the two different divergent slit settings used for the plutonium oxide samples. Perhaps more will be learned later if TEM can be incorporated into such a study. Also, the contrast factors calculated in this study as part of the defect analysis used single-crystal elastic constants that were obtained through density functional theory calculations. If revisions are made to the single-crystal elastic constants in the future, this could change the results obtained in this study, although probably not significantly, since there seemed to be little contribution to line profile broadening beyond the crystallite size effects.

Acknowledgements This research was supported by the Nuclear Process Science Initiative (NPSI) at Pacific Northwest National Laboratory (PNNL). PNNL is a multiprogram national laboratory operated for the U.S. Department of Energy (DOE) by Battelle Memorial Institute under Contract No. DE-AC05-76RL0-1830. PNNL-SA-141652.

References

Ashbee, K. H. G. & Frank, F. C. (1970). *The Philosophical Magazine: A Journal of Theoretical Experimental and Applied Physics* **21**, 211-213.
Belin, R. C., Valenza, P. J., Reynaud, M. A. & Raison, P. E. (2004). *J. Appl. Crystallogr.* **37**, 1034-1037.
Borbely, A., Dragomir-Cernatescu, J., Ribarik, G. & Ungar, T. (2003). *Journal of Applied Crystallography* **36**, 160-162.
Caglioti, G., Paoletti, A. & Ricci, F. P. (1958). *Nucl. Instrum.* **3**, 223.
Cheary, R. W. & Coelho, A. (1992). *Journal of Applied Crystallography* **25**, 109-121.
Cina, B. (1963). *J. Nucl. Mater.* **9**, 85-100.
Delegard, C. H. (2013). *Radiochim. Acta* **101**, 313-322.
Ectors, D., Goetz-Neunhoeffer, F. & Neubauer, J. (2015a). *Journal of Applied Crystallography* **48**, 189-194.
Ectors, D., Goetz-Neunhoeffer, F. & Neubauer, J. (2015b). *Journal of Applied Crystallography* **48**, 1998-2001.
Haschke, J. M., Allen, T. H. & Morales, L. A. (2000). *Science (Washington, D. C.)* **287**, 285-287.
Hixon, A. E. & Powell, B. A. (2018). *Environ. Sci.: Processes Impacts* **20**, 1306-1322.
Kanellakopulos, B., Dornberger, E., Muller, L., Baumgartner, F., Benedict, U. & Dufour, D. (1983). Institut fur HeiBe Chemie, Kernforschungszentrum Karlsruhe.
Kersting, A. B. (2013). *Inorg. Chem.* **52**, 3533-3546.
Kril, C. E. & Birringer, R. (1998). *Philosophical Magazine A* **77**, 621-640.
Krivoglaz, M. A. & Ryaboshapka, K. P. (1963). *Fiz. Met. Metalloved.* **15**, 18-31.
Leoni, M., Confente, T. & Scardi, P. (2006). *PM2K: A flexible program implementing Whole Powder Pattern Modelling*.
Leoni, M., Di Maggio, R., Polizzi, S. & Scardi, P. (2004). *J. Am. Ceram. Soc.* **87**, 1133-1140.
Machuron-Mandard, X. & Madic, C. (1996). *J. Alloys Compd.* **235**, 216-224.
Martinez-Garcia, J., Leoni, M. & Scardi, P. (2009). *Acta Crystallographica Section A* **65**, 109-119.
Mayer, K., Wallenius, M. & Varga, Z. (2013). *Chem. Rev. (Washington, DC, U. S.)* **113**, 884-900.
Mittemeijer, E. J., Scardi, P. & Editors (2004). *Diffraction Analysis of the Microstructure of Materials. [In: Springer Ser. Mater. Sci., 2004; 68]*. Springer-Veralg.
Runde, W., Brodnax, L. F., Goff, G., Bean, A. C. & Scott, B. L. (2009). *Inorg. Chem.* **48**, 5967-5972.
Scardi, P. & Leoni, M. (2001). *Acta Crystallographica Section A* **57**, 604-613.
Scardi, P. & Leoni, M. (2002). *Acta Crystallogr A* **58**, 190-200.
Scardi, P., Leoni, M. & Dong, Y. H. (2000). *Eur. Phys. J. B* **18**, 23-30.
Scardi, P., Leoni, M., Mueller, M. & Di Maggio, R. (2010). *Mater. Sci. Eng., A* **A528**, 77-82.
Scardi, P., Ortolani, M. & Leoni, M. (2010). *WPPM: Microstructural Analysis beyond the Rietveld Method*.
Scherrer, P. (1918). *Nachr. Ges. Wiss. Gottingen* 96-100.
Simmons, J. A., De Wit, R., Bullough, R., Research, I. f. M. & Standards, U. S. N. B. o. (1970). *Fundamental aspects of dislocation theory: conference proceedings, National Bureau of Standards, April 21-25, 1969*. U.S. National Bureau of Standards; for sale by the Supt. of Docs., U.S. Govt. Print. Off.
Smith, P. K., Burney, G. A., Rankin, D. T., Bickford, D. F. & Sisson, R. D., Jr. (1976). E. I. du Pont de Nemours and Co.
Snyder, R. L., Fiala, J., Bunge, H. J. & Editors (1999). *Defect and Microstructure Analysis by Diffraction. [In: Int. Union Crystallogr. Monogr. Crystallogr., 1999; 10]*. Oxford Univ Press.
TOPAS. (2016). Version 6.
Ungar, T. & Tichy, G. (1999). *Phys. Status Solidi A* **171**, 425-434.
Vella, A., Whitley, R. J., Armstrong, N. G., Dowd, A. R. & Cline, J. P. (2006). *Annual Condensed matter and materials meeting* 1-4.

Warren, B. E. (1969). *X-ray diffraction*. Reading, Mass.: Addison-Wesley Pub. Co.
Warren, B. E. & Averbach, B. L. (1950). *J. Appl. Phys.* **21**, 595-598.
Weber, W. J. (1984). *Radiat. Eff.* **83**, 145-156.
Wilkens, M. (1970). *physica status solidi (a)* **2**, 359-370.
Williamson, G. K. & Hall, W. H. (1953). *Acta Metall.* **1**, 22-31.
Zachariasen, W. H. (1949). *Acta Crystallogr.* **2**, 388-390.
Zhang, P., Wang, B.-T. & Zhao, X.-G. (2010). *Physical Review B* **82**, 144110.

Pacific Northwest National Laboratory

902 Battelle Boulevard
P.O. Box 999
Richland, WA 99354
1-888-375-PNNL (7665)

www.pnnl.gov